Journal of Transportation Technologies, 2025, 15(4), 560-577
https://www.scirp.org/journal/jtts
ISSN Online: 2160-0481
ISSN Print: 2160-0473

Non-Contact Acoustic Emission Detection of External Rail Defects Using Air-Coupled Sensors

Lei Jia[1], Jee Woong Park[1], Ming Zhu[2], Yingtao Jiang[2], Lihao Qiu[2], Hualiang Teng[1]

[1]Department of Civil and Environmental Engineering and Construction, University of Nevada, Las Vegas, NV, USA
[2]Department of Electrical and Computer Engineering, University of Nevada, Las Vegas, NV, USA
Email: jial5@unlv.nevada.edu, jee.park@unlv.edu, ming.zhu@unlv.edu, yingtao.jiang@unlv.edu, qiul1@unlv.nevada.edu, hualiang.teng@unlv.edu

How to cite this paper: Jia, L., Park, J.W., Zhu, M., Jiang, Y.T., Qiu, L.H. and Teng, H.L. (2025) Non-Contact Acoustic Emission Detection of External Rail Defects Using Air-Coupled Sensors. *Journal of Transportation Technologies*, **15**, 560-577.
https://doi.org/10.4236/jtts.2025.154026

Received: May 21, 2025
Accepted: October 19, 2025
Published: October 22, 2025

Abstract

Rail defects, both internal and external, pose significant safety risks. Acoustic Emission (AE) technology has emerged as a promising method for monitoring damage progression and detecting rail defects. This research aims to investigate AE signal characteristics generated from external rail defects using both rail-mounted and vehicle-mounted settings. This investigation is expected to enhance our understanding of how AE signals correlate with defects and how effectively they can identify them. The results of the tests revealed two key findings. First, the AE detection rate is low, which suggests that AE detection rates may depend heavily on defect size and field conditions. Second, wavelet packet power (WPP) analysis indicates that the AE signals from external rail defects exhibited concentrated and intense peaks within the 100 - 160 kHz range. Overall, detecting external defects showed low performance due to indistinct AE signal characteristics and significant environmental noise. However, the application of continuous wavelet transforms (CWT) and wavelet packet power analysis presented more insights by identifying energy distributions and frequency peaks associated with external defects.

Keywords

Railroad Infrastructure, Rail Defect Detection, Wavelet Analysis, Acoustic Emission Detection

1. Introduction

In railroad transportation, rail and wheels directly interact as trains move. The

rails experience wear and tear during daily operations, leading to both internal and external defects over time. As part of defect detection efforts, various inspection and detection technologies, including imaging and ultrasound detection, have been applied to monitor rail surface health conditions.

The optical imaging method is a recognition technology that uses graphics scanning and processing, with a high-speed, high-resolution camera. An optical encoder is used for graphics recognition and classification. Recent experimental research has demonstrated that optical systems can detect surface defects at speeds over 135 mph [1]. An automatic optical detecting system can detect flaws using color line-scan cameras and a spectral image differencing procedure [2]. This system is particularly advantageous for detecting minor defects, including invisible cracks, and automates about 95% of inspection work, significantly increasing inspection efficiency compared to previous techniques. Advanced optical technologies include a 3D laser profiling system (3D-LPS) [3]. This system uses a laser scanner, odometer, inertial measurement unit (IMU), and GPS to collect rail surface information. The primary challenges the system faces are several including but not limited to complex disturbance factors, limited recognition features, and limited capability to detect internal defects [4].

Electromagnetic techniques include eddy current testing (ECT) and alternative current field measurement methods (ACFM). ECT employs electromagnetic induction to inspect rail surfaces [5] [6]. Discontinuities on the rail surface affect the magnitude of the eddy current, and the detector recognizes these changes based on collected data. Studies have shown that ECT can be used effectively at high-speed rails up to 90 km/h. However, it requires close proximity to the rail surface and is highly sensitive to variations in the lift-off distance, posing a challenge when considering real-world applications. ACFM measures magnetic field disturbances to size surface-breaking cracks [7]. This technology does not require direct electrical contact with the surface and can operate across various environments. Research results from various simulated defect conditions suggest ACFM is accurate and reliable for detecting surface-breaking defects at speeds over 150 mph [7] [8]. The results confirmed that the ACFM sensor could identify visible cracks as small as 1.2 mm.

Magnetic-related techniques, such as electromagnetic tomography technology (EMT), are less commonly utilized in rail defect detection methods [9]. This technology uses a tomographic approach to measure the alternating magnetic signal modulated by cracks in the rail and then reconstructs their distribution. A key advantage is its ability to detect and reconstruct internal cracks within the rail, offering a non-contact, continuous inspection method that can operate at higher speeds compared to traditional inspection techniques. However, EMT systems are expensive and require specialized expertise to operate the equipment. The system's complexity demands professional knowledge for the proper use and interpretation of the equipment, making it less accessible than other standard inspection methods. Additionally, the non-encircling sensor structure of EMT must be

adapted to the mechanical constraints of rail tracks, such as rail bed mounting clips and turnout junctions, which can complicate sensor installation.

AE is an elastic wave generated by changes in the material's internal structure, typically caused by a sudden change in internal stress or external impacts [10] [11]. These changes can involve crack growth, material displacement, phase changes, fiber breakage, or decomposition. When AE signals are generated due to elastic deformation, sensors respond to the dynamic motion and collect the signals. In recent years, optical microphones have gained attention for their innovative technology and superior performance in non-contact ultrasonic detection. The nature of air-coupled AE waves makes it feasible to develop non-contact sensors for detecting rail defects using this technology. As shown in **Figure 1** [12], when a monochromatic laser beam propagates through a medium in the presence of a sound field, it experiences slight modulation in its optical wavelength. This modulation is proportional to the local density and, consequently, the sound pressure. The core component of the optical microphone is a miniaturized Fabry-Perot cavity consisting of two semi-reflective mirrors. The intensity of the laser light reflected from this cavity is determined by the product of the input intensity and a transfer function. The round-trip phase shift depends on the laser wavelength and the distance between the mirrors. Therefore, any change in the laser wavelength induced by the sound field alters the light intensity, which is reflected by the cavity and can be detected by a photodiode.

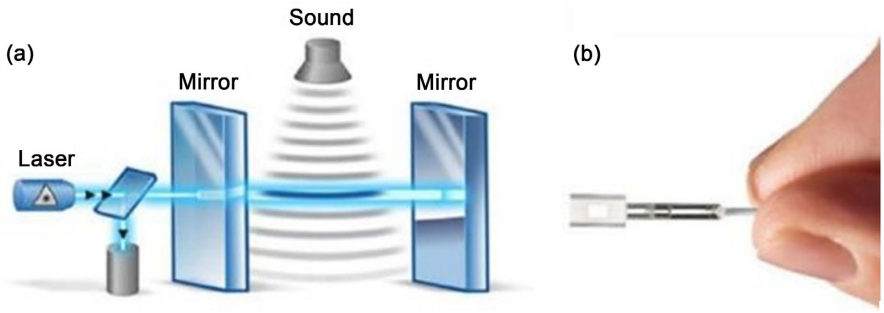

Figure 1. The optical microphone: (a) Mechanism; (b) Sensor head [12].

Unlike the bone-conduction sensors, this non-contact approach utilizes air-couple sensors to record AE signals. Traditional piezoelectric ultrasonic sensors generally work within a narrow frequency bandwidth (±10% of the resonate frequency). The optical microphone is introduced in this approach to address this limitation. The key question is whether the optical microphone sensor can detect external defects located far from the sensor.

This study explores the AE characteristics of acoustic emission generated from external defects and evaluates the performance of the air-coupled sensor in detecting external defects in real-world field tests. The tests involve external defects at two locations, with follow-up analysis and evaluations focusing on the characteristics of the AE signals. The study provides insights into the effectiveness and

current limitations of this approach for railroad health inspection.

2. Methodology

As highlighted in the previous sections, AE testing offers a promising approach for detecting defects in rail structures due to its ability to capture real-time stress-related events without requiring direct mechanical contact. AE techniques are particularly valuable because they are sensitive to dynamic processes, such as crack initiation, crack growth, and surface fatigue—key concerns in rail infrastructure. Unlike conventional non-destructive testing methods, which often require point-by-point inspection or close proximity to defects, AE allows for remote monitoring of large areas, making it well-suited for field applications where access is limited, or continuous inspection is necessary.

For external rail defects, detecting AE signals can be especially challenging because such defects often produce weaker emissions compared to internal cracks. Nevertheless, understanding AE signal behavior under realistic conditions is critical for developing effective detection methods. Therefore, this study investigates how AE signals propagate from external defects in rail systems and evaluates the factors affecting signal attenuation and detection capability.

2.1. Technical Background of AE

The complexity of AE signals is primarily influenced by two factors: the characteristics of the source and the propagation path. The source characteristics are determined by the defect type and material properties, while the propagation characteristics are largely influenced by structural dimensions. In AE applications, sensors are commonly deployed to detect potential defects within structures across distances that range from a few to over ten meters.

AE energy attenuation during propagation is influenced by several factors: geometric spreading, interior friction, scattering, and diffraction [13].

- Geometric spreading causes the signal amplitudes to decrease as waves originating from a single spot expand over a broader area. In three-dimensional solids, the wave amplitude (A) diminishes inversely with distance d, that is $A \propto 1/d$. In two-dimensional solids, it decreases inversely with the square root of distance, that is $A \propto 1/\sqrt{d}$.
- Internal friction is a process where mechanical energy is converted to thermal energy as waves travels through non-conservative media, contributing to further amplitude reduction. This material-dependent effect causes amplitude to decay with distance $A \propto e^{-kd}$, in which k denotes the attenuation coefficient.
- Scattering and diffraction occur when waves encounter boundaries, such as cavities. Scattering usually occurs when the waves interact with finite voids, while diffraction take place at sharp edges. Both result in additional amplitude reduction.

In general, near the AE source, attenuation is dominated by geometry spreading. At greater distances from the AE source, internal friction becomes more im-

portant, becoming the primary cause of signal decay, following exponential attenuation over distance. In contrast, dispersion plays a limited role under typical conditions. The AE signal attenuation behaviors have been investigated through controlled tests, such as placing sensors at varying distances from an AE source.

AE wave modes are influenced by different boundaries, generating different waves such as body and surface waves [14].

- Body waves generally propagate in infinite media and include longitudinal waves (with particle motion parallel to wave travel direction) and transverse waves (with particle motion perpendicular to wave direction). Longitudinal waves generally have the highest velocity.
- Surface wave, such as Rayleigh wave, is another wave type that travels along the surfaces of semi-infinite media or thick solids, penetrating approximately one wavelength into the material. Combining longitudinal and transverse motion, these waves travel at speeds slightly below shear waves, depending on material elasticity.

In addition to these, plate waves, primarily Lamb waves, are confined to thin structures like plates. Lamb waves exhibit multiple modes categorized into symmetric (extensional) and anti-symmetric (flexural) types, with in-plane and out-of-plane motion. These characteristics, however, may not hold consistently at higher frequencies. Guided waves propagate along elongated structures, such as plates, pipes, and rails, constrained by boundaries [15]. Although terms like "guided Rayleigh waves" and "guided Lamb waves" better describe the practical conditions, these modes allow long-distance wave travel with minimal energy loss, making them suitable for long-range ultrasonics in rail condition monitoring.

2.2. Testing Prototype

The testing prototype is shown in **Figure 2**. The prototype developed included data acquisition equipment, optical microphone sensors, pre-amplifiers, and high-speed cameras. Membrane-free Optical Microphone model Eta 250 was used in this study. The frequency range is 10 Hz - 1 MHz, dynamic range is 100 dB; and self-noise is 50 μPa. National Instrumental cRio 9041 with module NI 9223 were utilized as data acquisition (DAQ) equipment, the sampling rate was 1 MHz. Mistras 2/4/6 voltage preamplifiers (PAC 2/4/6) were employed to amplify the AE signals before they were recorded by DAQ equipment. The gain was set to 60 dB for all the tests to ensure the AE signal qualities. During the test, the band-pass filter was selected to be 20 - 500 kHz to eliminate the effects of low-frequency noises unrelated to the AE events. Labview was used to control data collection and storage. To ensure long-time data recording without interruption, the producer and consumer modules were employed to save current data and keep recording new data simultaneously. A go-pro camera was utilized to record geo-information during the field tests. It provides up to 240 frames video recording. Hammer hit was employed when each test started, to synchronize the time between video and AE signals.

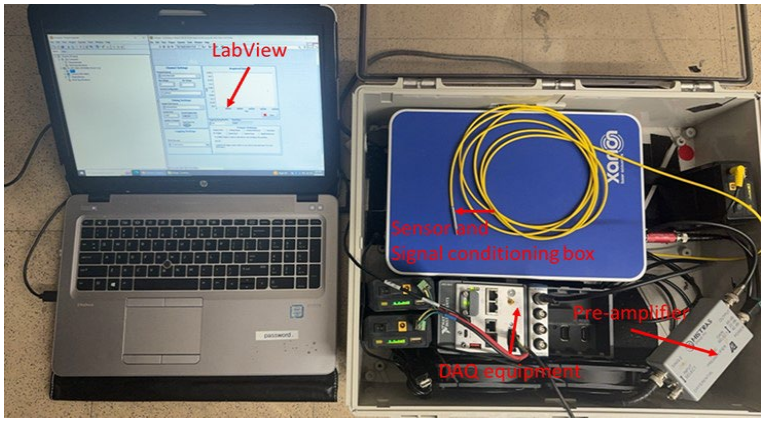

Figure 2. DAQ system schematic.

2.3. Rail External Defect Detection in Nevada Railroad Museum

2.3.1. Rail-Mounted Field Test

Two external defects were utilized in this test, and the locations were as presented in **Figure 3**. There were excursion trains operated on the tracks in the Museum. The defects were measured by visual inspection, as presented in **Figure 4**. The sensor head was mounted near the rail head. Two testing scenarios were evaluated in this test:

1) The sensor was moved vertically away from the railhead.

2) The sensor was positioned below the railhead and moved horizontally along it.

The first case adjusted the sensor placement across three different locations as shown in **Figure 5(a)** by moving it away from the defect by one inch in the subsequent test. The second case adjusted the sensor placement in three different locations as shown in **Figure 5(b)** by moving it two inches to the left during each subsequent test.

An unloaded hopper car, with an axle load of approximately 70,000 lb., was employed. The tests were conducted at 5 mph. A GoPro camera was installed near these defect sites to record when the wheel passed over the defects. A hammer hit was used to synchronize the video and AE signal timeline, allowing precise analysis of AE events and associated noises.

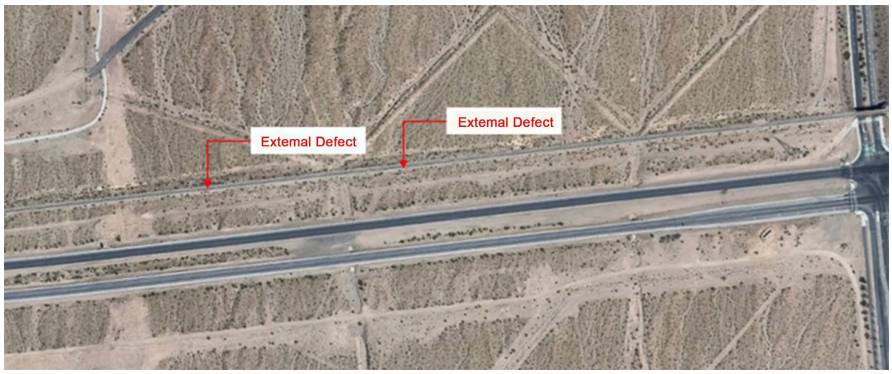

Figure 3. Location of two external defects in the Nevada Railroad Museum (google map).

(a) Surface defect 1: 1.3 in*0.7 in (b) Surface defect 2: 1.2 in*0.5 in

Figure 4. External defect location and size.

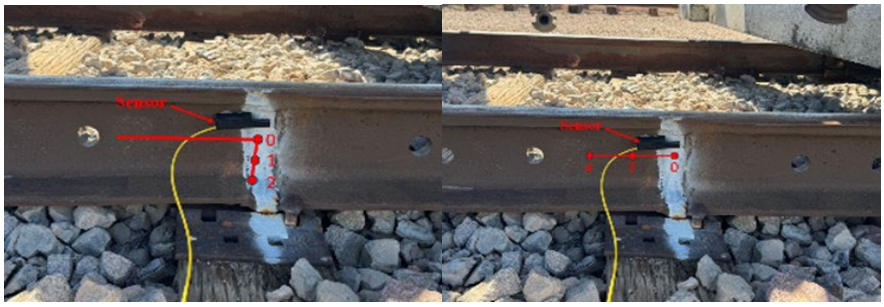

(a) (b)

Figure 5. Attenuation evaluation (a) Vertically in the air; (b) Longitudinally in the rail.

2.3.2. Vehicle-Mounted Field Test

In this testing scenario, the sensor was installed on the train's mounting frame, and acoustic signals were recorded when the train was running over defects (**Figure 6**). The sensor was safely placed 1.5 inches away from the rail head side to ensure safety. During testing, the sensor was relocated from its original position to the far side of the defect by moving it at a two-inch increment on each subsequent test (**Figure 7**). The covered distances were 0, 2, and 4 inches farther from the defect site.

(a) (b)

Figure 6. Mounting frame (front and side views).

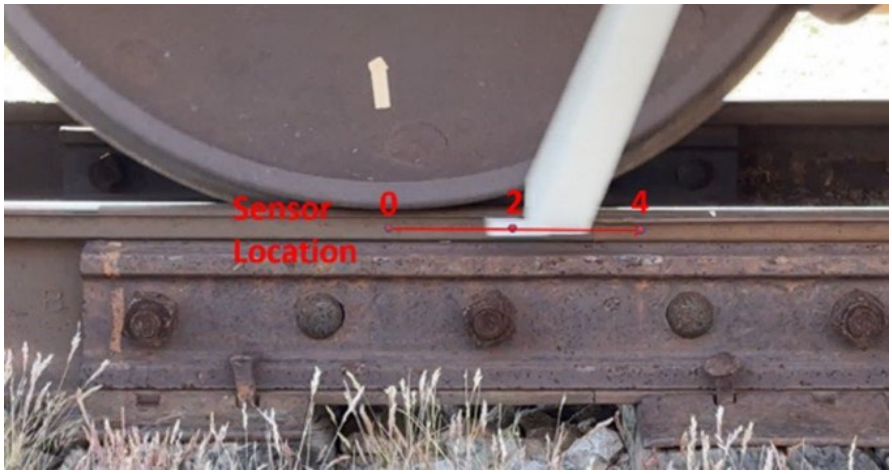

Figure 7. Attenuation evaluation in the rail (longitudinally).

2.4. Rail External Defect Detection in MxV Rail

The tests conducted in Nevada provided valuable preliminary insights into external defect detection. However, further evaluation was necessary because the external defects identified at the museum were based solely on visual inspection. To address this, additional field tests were conducted at MxV Rail in Colorado, targeting defects confirmed through more rigorous inspection methods. Regular freight trains were operated on the track. The type and the size of the defects are similar to those in Figure 4. Two test scenarios were originally planned: 1) rail-mounted testing and 2) vehicle-mounted testing, with the external defect located near the main entry of the MxV Rail FAST loop (Figure 8).

During the field testing, unforeseen damage to the sensor head occurred, which led to the cancellation of the rail-mounted tests. As a result, only the vehicle-mounted tests were completed.

Figure 8. Location of the external defect in the MxV rail (google map).

Vehicle-Mounted Field Test

In this testing scenario, the sensor was installed the same configuration used during the Nevada tests. It was installed on the train's mounting frame, and the acoustic signals were recorded when the train was running over defects (Figure 6). The sensor was safely placed 1.5 inches away from the rail head side to ensure safety.

During testing, the sensor was relocated from its original position to the far side of the defect by moving it at a two-inch increment on each subsequent test (**Figure 7**). The covered distances were 0, 2, and 4 inches farther from the defect site.

2.5. Time-Frequency Representation of AE Signals

For accurate characterization of AE signals, especially those signals change over time, it is essential to process and present signals effectively. Non-stationary signals, whose frequencies and amplitudes vary with time, pose a particular challenge for traditional methods like the Fourier transform. While the Fourier transform provides a global view of the frequency components, it can fail to capture localized variations in time. In contrast, time-frequency analysis, particularly wavelet techniques, offers significant advantages in this aspect [16]. Wavelet transforms, such as continuous wavelet transform (CWT) and discrete wavelet transform (DWT), enable multi-resolution analysis of signals, effectively capturing both time and frequency information.

In this study, the CWT is utilized instead of DWT due to its ability to operate at narrower scales, offering enhanced multi-resolution capabilities and superior performance in noisy environments, particularly for detecting discontinuity. To minimize computational effort, the analysis is conducted on specific segments of AE waves.

Based on the definition, CWT is the convolution of the signal $x(t)$ with a set of wavelet functions $\psi_{a,b}(t)$ which are created by dilating and translating a single mother wavelet $\psi(t)$ that meets certain criteria [17] [18].

$$WT(a,b) = \int_{-\infty}^{\infty} x(t)\psi_{a,b}^{*}(t)\mathrm{d}t \tag{1}$$

where,

$$\psi_{a,b}(t) = \frac{1}{\sqrt{a}}\psi\left(\frac{t-b}{a}\right)\left(a,b \in R, \text{and } a > 0\right) \tag{2}$$

In the equation above, $\psi_{a,b}(t)$ represents the complex conjugate, a denotes the scale parameter, b indicates the translation parameter, t is the time, and $WT(a,b)$ is the wavelet coefficient associated with it. The wavelet function $\psi_{a,b}(t)$ is centered at b with a spread proportional to a, which is calculated as a window function in the time-frequency domains. During the transform, a series of $\psi_{a,b}(t)$ is produced based on multiple values of a and b. The selection of the mother wavelet greatly impacts the outcomes of CWT. Therefore, it is essential to determine an appropriate mother wavelet based on various aspects of wavelets (such as symmetry, orthogonality, and support size).

An appropriate mother wavelet is essential to the results of CWT analysis. Various components need to be considered before selecting the optimized mother wavelet. In this study, the complex Morlet wavelet was utilized due to its remarkable time-frequency domain resolution [19] [20]. The function and its corresponding Fourier transform are,

$$\psi(t)=\frac{1}{\sqrt{\pi f_b}}\exp(i2\pi f_c t)\exp\left(-\frac{t^2}{f_b}\right) \tag{3}$$

$$\hat{\psi}(f)=\exp\left\{-\pi^2 f_b (f-f_c)^2\right\} \tag{4}$$

Here, f_b denotes the non-dimensional bandwidth parameter, f_c denotes the wavelet central frequency in Hz, and i represents the imaginary unit. Additionally, f_b and f_c need to be selected based on the analyzed AE signals. In general, the Morlet wavelet is suggested $f_c \geq 5/2\pi$ due to the rapid attenuation in the envelope. Shannon entropy can be utilized to quantify the entropies in order to determine the proper parameters of the mother wavelet, such as f_b and f_c. It indicates the similarity between the basis function and the signal being analyzed. A lower wavelet entropy value signifies a greater similarity, making it a useful criterion for selecting the appropriate basis function for the wavelet transform. In this study, $f_b=0.5$ and $f_c=4$ were selected in this study to ensure the lowest wavelet entropy [21].

2.6. Wavelet Packet Power-Based AE Identification

Wavelet Power is a method used to analyze the energy distribution of signals across different frequency bands by decomposing the signal into components at various scales [20]. The wavelet transform provides a time-frequency representation of a signal, allowing detailed analysis of transient and non-stationary phenomena. However, a limitation of the standard wavelet transform is its unequal frequency resolution: it offers good time resolution and poor frequency resolution at high frequencies, and good frequency resolution with poor time resolution at low frequencies. This characteristic is due to the nature of the wavelet transform's multiresolution approach, where only approximation coefficients (lower frequency components) are further decomposed at each level. In general, for a signal $x(t)$, the wavelet coefficients at scale j and position k are given by:

$$W(j,k)=\int x(t)\psi_{j,k}(t)\mathrm{d}t \tag{5}$$

where $\psi_{j,k}$ is the wavelet function scaled by j and translated by k. The wavelet power at each scale can be represented as:

$$P_j=\left|W(j)\right|^2 \tag{6}$$

However, this traditional approach does not maintain consistent resolution across all frequency bands. To overcome the limitations of the wavelet transform, the Wavelet Packet Transform (WPT) was developed. Unlike the traditional wavelet transform, WPT decomposes both approximation and detail coefficients at each level, resulting in a more uniform resolution across all frequency scales. This means that WPT provides enhanced frequency resolution even at higher frequencies, making it more suitable for analyzing signals with complex frequency content, such as AE waves. In WPT, the decomposition is performed on both the approximation and detail coefficients using recursive filtering and down sam-

pling, defined as:

$$wp(i+1,2j)=\sum_{n} h[n]\cdot wp(i,j)[2n] \tag{7}$$

$$wp(i+1,2j+1)=\sum_{n} g[n]\cdot wp(i,j)[2n] \tag{8}$$

where $h[n]$ and $g[n]$ are the low-pass and high-pass filter coefficients, respectively. This process results in a full binary tree structure, where each node represents a frequency band, and the nodes at each level correspond to different scales with consistent resolution. The Wavelet Packet Power (WPP) for each frequency scale i can then be calculated as the squared magnitude of the wavelet packet coefficients:

$$P_{i,j}=\left|wp(i,j)\right|^2 \tag{9}$$

To summarize the energy distribution across scales, the maximum WPP for each scale i is expressed as:

$$\mathrm{WPP}_i=\max\left\{\left|wp(i,j)\right|^2\right\}, j=1,2,\cdots,M \tag{10}$$

In this study, WPT-based power analysis was utilized to exploit the advantage of uniform frequency resolution across all scales, which is particularly beneficial for accurately capturing and analyzing AE signals. This approach allows for a detailed examination of energy distribution across frequency bands, aiding in the identification and characterization of AE sources with improved precision.

To ensure the data quality in presenting the AE characteristics, all the WPP calculations were performed using the signals collected at 0 inch for all the scenarios. A high-pass filter with a cutoff frequency of 100 kHz was applied to the data to better evaluate the AE characteristics in high-frequency range.

3. Results and Discussion

Two stages of field tests were conducted to evaluate AE signal propagation and attenuation characteristics under various conditions, specifically targeting external defects in rail structures (Table 1). The first stage involved field tests at the Nevada Railroad Museum, focusing on an initial evaluation of AE signal characteristics in a real-world environment. Both rail-mounted and vehicle-mounted configurations were used, with sensor offsets at 0, 2, and 4 inches for rail-based measurements and 0, 1, and 2 inches for air-based measurements. Each configuration was repeated 10 times. The weather when the tests were performed was excellent. The second stage took place at the MxV Rail facility for further evaluation, building on findings from the Nevada tests. Similar sensor configurations were used, with identical offsets and repetition counts to allow for a consistent and thorough evaluation of AE signal behavior under different testing environments. The weather was clear when the tests were performed. Note that all the rail-mounted tests were canceled due to the sensor damage.

Table 1. Summary of external defect tests.

Test Location	Sensor Location	Attenuation Evaluated	Test Speed (mph)	Offset From Defect	Number of Repeats	Goal
Nevada	Rail-mounted	Rail	5	0, 2, 4	10 each	Initial evaluation of AE signals
		Air	5	0, 1, 2	10 each	
	Vehicle-mounted	Rail	5	0, 2, 4	10 each	
MxV Rail	Rail-mounted	Rail	5	0, 2, 4	Canceled	Further evaluation of AE signals
		Air	5	0, 1, 2		
	Vehicle-mounted	Rail	5	0, 2, 4	10 each	

3.1. Time-Frequency Representation of Defect Signals

The AE signals collected from the defect areas during the field tests were analyzed using the Continuous Wavelet Transform (CWT). In the Nevada field tests, CWT analysis did not reveal clear AE signals. As shown in Figure 9, the tests predominantly captured low-frequency mechanical vibrations throughout the entire testing period.

In the MxV Rail field test, only two AE events were detected by the sensor during the examination of external defects, as illustrated in Figure 10 and Figure 11. The observed patterns primarily featured low-frequency components that dominate the energy spectrum, with notable energy peaks concentrated in the 120 - 150 kHz range. Several factors may explain these observations:

- The external defects in Nevada may have entered into stable conditions, producing minimal active crack growth and thus few AE signals.
- The defect at MxV Rail may have been at an early stage, generating very limited AE activity.

Additional field tests are necessary to better assess the feasibility of using AE methods for detecting external rail defects and to further validate the effectiveness of AE signal analysis under real-world field environments.

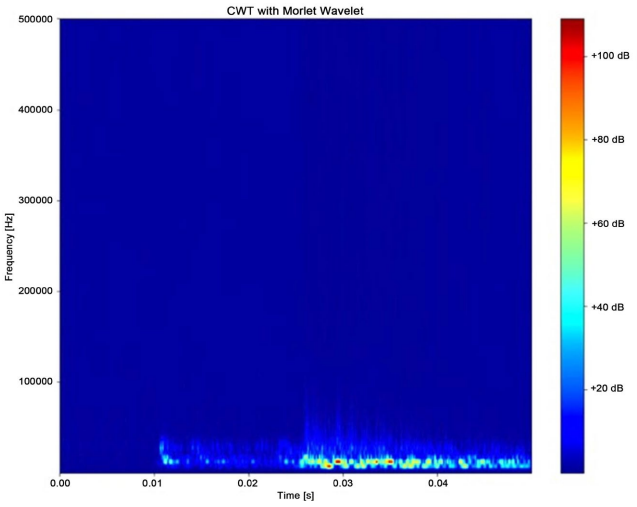

(a)

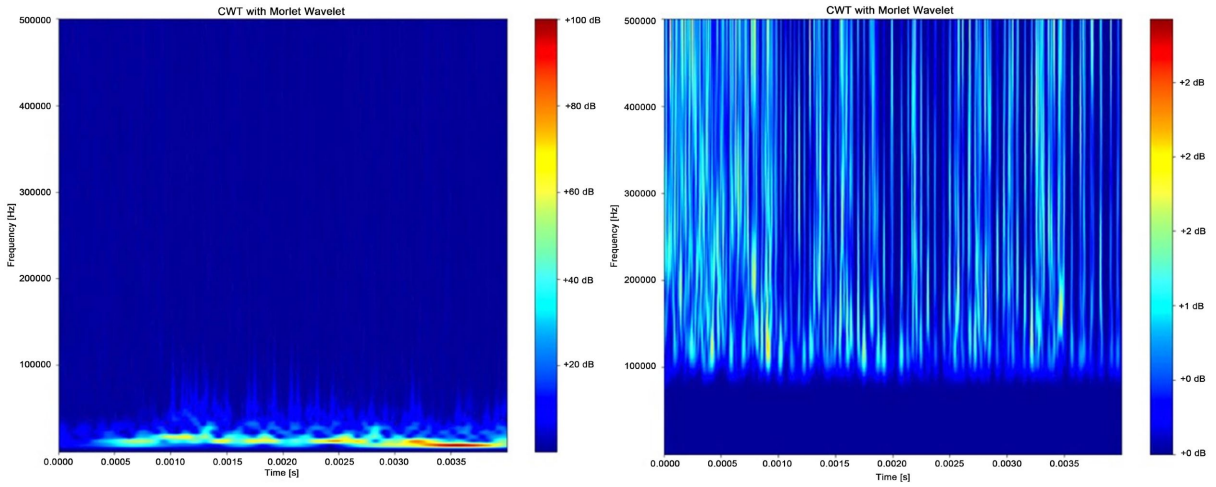

(b) (c)

Figure 9. CWT of AE in Nevada (a) Overview; (b) 20 kHz filter; (c) 100 kHz filter.

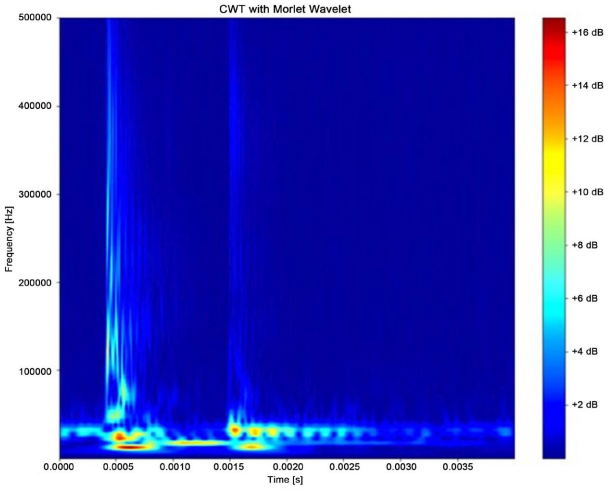

(a)

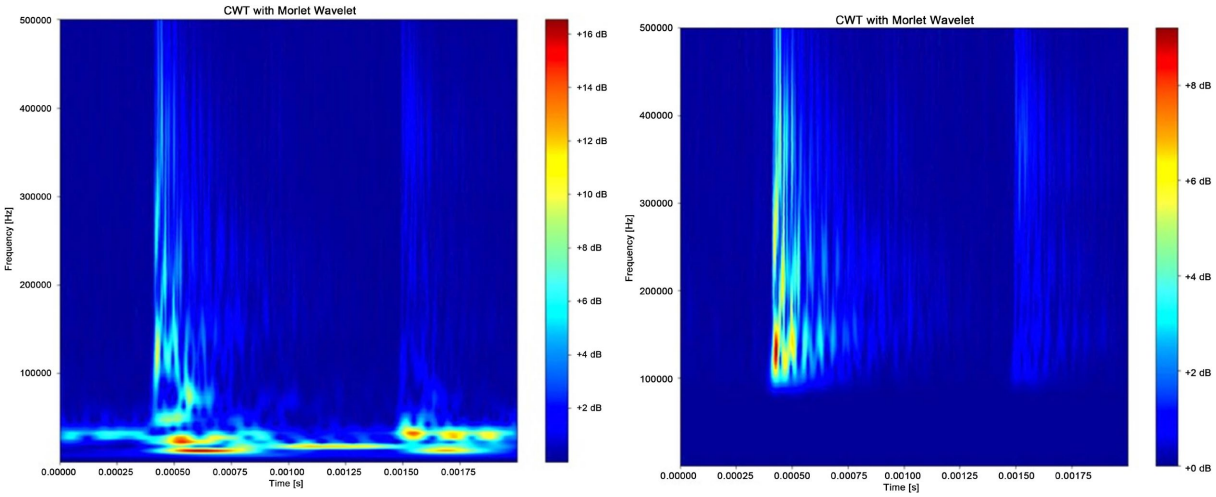

(b) (c)

Figure 10. CWT of AE (1) in MxV Rail (a) Overview; (b) 20 kHz filter; (c) 100 kHz filter.

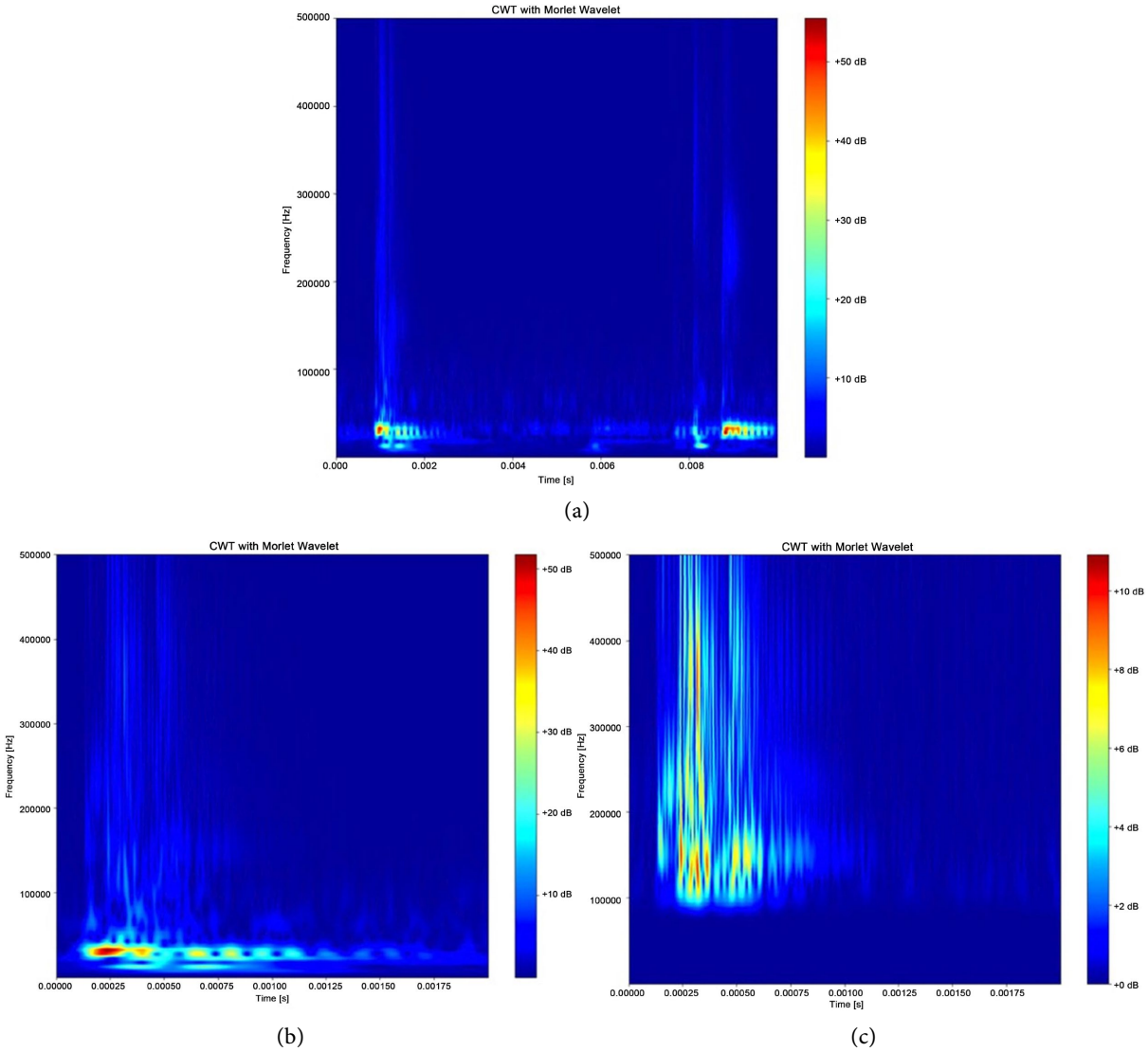

Figure 11. CWT of AE (2) in MxVRail (a) Overview; (b) 20 kHz filter; (c) 100 kHz filter.

3.2. Wavelet Packet Power (WPT)-Based AE Identification

The AE events captured in MxV Rail were further analyzed using WPT-based power analysis. The WPP calculations were performed on the two signals collected at the 0-inch offset position for the MxV Rail surface defects. To better evaluate the AE characteristics in high-frequency ranges, a high-pass filter with a cutoff frequency of 100 kHz was applied to all the data. As shown in Figure 12, the WPP spectra and its corresponding maxima illustrate the typical energy distribution of the field-collected signals. The power spectra indicates that the energy is concentrated primarily within the 100 kHz-to-400 kHz frequency range. It also shows three prominent energy peaks around 100 - 140 kHz, 200 kHz, 280 kHz, and 360 kHz. These frequency peaks appeared consistently in both plots, suggesting common features likely related to the AE characteristics of the external rail defects.

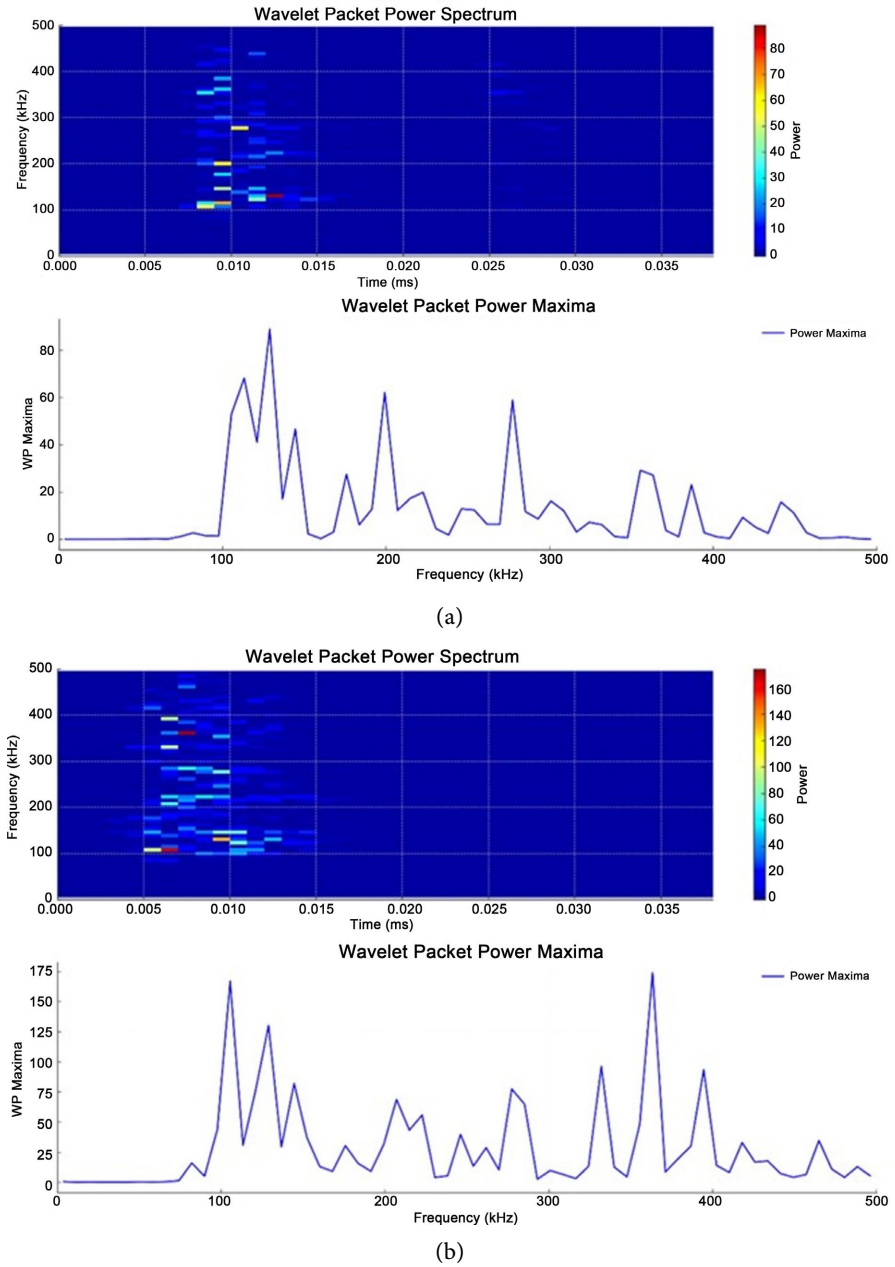

Figure 12. WPP spectrum and maxima of defect-induced AE signals.

4. Conclusions and Recommendations

AE signal characteristics were evaluated through real-world field tests. The results demonstrated the potential of the developed method to detect external defects, although some limitations were observed due to environmental noise and signal attenuation. External defects, such as those caused by wear and fatigue, present distinct challenges because their damage mechanisms differ from those of internal defects, necessitating the development of advanced algorithms for noise isolation and defect identification.

Preliminary evaluations using CWT and WPP analysis revealed that AE signal

propagation characteristics vary significantly depending on testing conditions. These analysis methods helped identify typical energy distributions and frequency peaks associated with external defects, which are expected to play a crucial role in refining defect detection algorithms.

However, the study encounters challenges in detecting external-induced AE signals, mainly due to the limited number of AE events and significant ambient noise. It is recommended that future research focuses on enhancing defect identification algorithms and optimizing field testing setups to effectively isolate AE events from noise. XARION Laser Acoustics GmbH has a series of products: Eta 250, Eta 450 and Eta 600, each with increased accuracy of measurements in terms of frequency range, self-noise, maximum sound pressure and dynamic range. This study used Eta 250. Using advanced sensors is recommended for the study in future.

Moreover, the study also suggests that defects originating from external sources, such as wear and fatigue, may not follow the same growth patterns as internal cracks. Their development is often expanded by specific incidents like severe friction during braking or starting. Surface defects often develop over broad areas rather than concentrating at a single point, as is typical for internal defects. This distribution complicates defect identification, as AE signals can originate from any location within the fatigue and wear zones.

These findings highlight the need for more sophisticated algorithms capable of isolating true AE events from ambient noise and scattered emissions. The insights gained from this study are valuable for guiding future improvements in testing strategies (e.g., testing setups) and enhancing defect identification methods in rail systems.

Many factors influence the low detection rate, one of which is train speed. For safety reasons, the tests in this study were restricted at 5 mph which is much lower than the speed a regular train is operated in the field. It can be perceived that the impact on the rail by the wheel would be much more significant with trains running at higher speed. The detection rate could be very high, correspondingly. The sensors can be placed on a maintenance inspection vehicle or regular trains that run at regular speed. The surface defects could be detected at least once when multiple times the train with sensors run over the defects.

The structure of the track influences the impacts of detection rate as well. Obviously, the impacts from heavy train on tracks with concrete ties are bigger than those on tracks with wooden ties. The corresponding detection rate could be quite different consistently.

Conflicts of Interest

The authors declare no conflicts of interest regarding the publication of this paper.

References

[1] Li, Q. and Ren, S. (2012) A Real-Time Visual Inspection System for Discrete Surface

Defects of Rail Heads. *IEEE Transactions on Instrumentation and Measurement*, **61**, 2189-2199. https://doi.org/10.1109/tim.2012.2184959

[2] Deutschl, E., Gasser, C., Niel, A. and Werschonig, J. (2004) Defect Detection on Rail Surfaces by a Vision Based System. *IEEE Intelligent Vehicles Symposium*, 2004, Parma, 14-17 June 2004, 507-511. https://doi.org/10.1109/ivs.2004.1336435

[3] Xiong, Z., Li, Q., Mao, Q. and Zou, Q. (2017) A 3D Laser Profiling System for Rail Surface Defect Detection. *Sensors*, **17**, Article 1791. https://doi.org/10.3390/s17081791

[4] Office of Railroad Policy and Development (2011) Rolling Contact Fatigue: A Comprehensive Review. https://railroads.dot.gov/sites/fra.dot.gov/files/fra_net/89/TR_Rolling_Contact_Fatigue_Comprehensive_Review_final.pdf

[5] Thomas Heckel, H.M.T., Kreutzbruck, M. and Rühe, S. (2009) High Speed Non-Destructive Rail Testing with Advanced Ultrasound and Eddy-Current Testing Techniques. https://www.ndt.net/article/Prague2009/ndtip/proceedings/Heckel_10.pdf

[6] Thomas, H., Heckel, T. and Hanspach, G. (2007) Advantage of a Combined Ultrasonic and Eddy Current Examination for Railway Inspection Trains. *Insight—Non-Destructive Testing and Condition Monitoring*, **49**, 341-344. https://doi.org/10.1784/insi.2007.49.6.341

[7] Papaelias, M.P., Roberts, C., Davis, C.L., Blakeley, B. and Lugg, M. (2010) Further Developments in High-Speed Detection of Rail Rolling Contact Fatigue Using ACFM Techniques. *Insight—Non-Destructive Testing and Condition Monitoring*, **52**, 358-360. https://doi.org/10.1784/insi.2010.52.7.358

[8] Sadeghi, F., Jalalahmadi, B., Slack, T.S., Raje, N. and Arakere, N.K. (2009) A Review of Rolling Contact Fatigue. *Journal of Tribology*, **131**, Article ID: 041403. https://doi.org/10.1115/1.3209132

[9] Liu, Z., Li, W., Xue, F., Xiafang, J., Bu, B. and Yi, Z. (2015) Electromagnetic Tomography Rail Defect Inspection. *IEEE Transactions on Magnetics*, **51**, 1-7. https://doi.org/10.1109/tmag.2015.2430283

[10] Bruzelius, K. and Mba, D. (2004) An Initial Investigation on the Potential Applicability of Acoustic Emission to Rail Track Fault Detection. *NDT & E International*, **37**, 507-516. https://doi.org/10.1016/j.ndteint.2004.02.001

[11] Nivesrangsan, P., Steel, J.A. and Reuben, R.L. (2007) Source Location of Acoustic Emission in Diesel Engines. *Mechanical Systems and Signal Processing*, **21**, 1103-1114. https://doi.org/10.1016/j.ymssp.2005.12.010

[12] Rohringer, W., Heine, T., Sommerhuber, R., Lehmann, N. and Fischer, B. (2018) Optical Microphone as Laser-Ultrasound Detector. https://www.optoscience.com/our-vendors/xarion/qip10g0000007jja-att/XARION_DAGA_2018.pdf

[13] Nazarchuk, Z., Skalskyi, V. and Serhiyenko, O. (2017) Acoustic Emission. Springer. https://doi.org/10.1007/978-3-319-49350-3

[14] Scruby, C.B. (1987) An Introduction to Acoustic Emission. *Journal of Physics E: Scientific Instruments*, **20**, 946-953. https://doi.org/10.1088/0022-3735/20/8/001

[15] Rizzo, P. and Coccia, S. (2009) Noncontact Rail Monitoring by Ultrasonic Guided Waves. In: Rizzo, P. and Coccia, S., Eds., *Encyclopedia of Structural Health Monitoring*, John Wiley & Sons, 2397. https://doi.org/10.1002/9780470061626.shm041

[16] Zhang, X., Feng, N., Wang, Y. and Shen, Y. (2015) Acoustic Emission Detection of Rail Defect Based on Wavelet Transform and Shannon Entropy. *Journal of Sound*

and Vibration, **339**, 419-432. https://doi.org/10.1016/j.jsv.2014.11.021

[17] Peng, Z.K. and Chu, F.L. (2004) Application of the Wavelet Transform in Machine Condition Monitoring and Fault Diagnostics: A Review with Bibliography. *Mechanical Systems and Signal Processing*, **18**, 199-221. https://doi.org/10.1016/s0888-3270(03)00075-x

[18] Yan, R., Gao, R.X. and Chen, X. (2014) Wavelets for Fault Diagnosis of Rotary Machines: A Review with Applications. *Signal Processing*, **96**, 1-15. https://doi.org/10.1016/j.sigpro.2013.04.015

[19] Teolis, A. (2017) Computational Signal Processing with Wavelets. Birkhäuser. https://doi.org/10.1007/978-3-319-65747-9

[20] Dehghan Niri, E. and Salamone, S. (2012) A Probabilistic Framework for Acoustic Emission Source Localization in Plate-Like Structures. *Smart Materials and Structures*, **21**, Article ID: 035009. https://doi.org/10.1088/0964-1726/21/3/035009

[21] Li, D. (2018) Rail Crack Monitoring Using Acoustic Emission Technique. Springer. https://doi.org/10.1007/978-981-10-8348-8